calculated and measured average Grüneisen parameters for some interactions are attributed to the inability of the simplified model to account appropriately for elastic and anharmonic anisotropy.

ACKNOWLEDGMENTS

The authors wish to thank the Computing Center of the Ministry of Mines and Hydrocarbons for the free use of its computing facilities during the course of this work. They are indebted to Dr. G. Bemski for reading the manuscript. They also thank R. Jiménez for his assistance in the construction of the cryostat.

[1]H. J. Maris, Phil. Mag. 9, 901 (1964).

[2]M. F. Lewis and E. Patterson, Phys. Rev. 159, 703 (1967).

[3]P. J. King, J. Phys. C 3, 500 (1970).

[4]R. C. Purdom and E. W. Prohofsky, Phys. Rev. B 2, 551 (1970).

[5]L. Landau and G. Rumer, Physik Z. Sowjetunion 11, 18 (1937).

[6]Valpey Corporation, Holliston, Mass.

[7]Matec, Inc., Providence, R.I.

[8]Solitron Devices, Inc., Rivera Beach, Fla.

[9]H. J. McSkimin, P. Adreatch, and R. N. Thurston, J. Appl. Phys. 36, 1624 (1965).

[10]R. N. Thurston, H. J. McSkimin, and P. Andreatch Jr., J. Appl. Phys. 37, 267 (1966).

[11]O. L. Anderson, J. Phys. Chem. Solids 24, 909 (1963).

[12]J. Lamb and J. Richter, Proc. Roy. Soc. (London) A293, 479 (1966).

[13]J. M. Ziman, Electrons and Phonons (Oxford U.P., New York, 1958), p. 60.

[14]Reference 13, p. 59.

[15]R. Nava, R. Callarotti, H. Ceva, and H. Martinet, Phys. Rev. 185, 1177 (1969).

[16]K. Brugger, Phys. Rev. 137, A1826 (1965).

[17]T. M. Fitzgerald and B. D. Silverman, Phys. Status Solidi 27, 473 (1968).

[18]M. G. Holland, Phys. Rev. 132, 2461 (1963).

[19]R. Berman, E. L. Foster, and J. M. Ziman, Proc. Roy. Soc. (London) A237, 344 (1956).

Determination of the Elastic Constants of Xenon Single Crystals by Brillouin Scattering*

W. S. Gornall[†] and B. P. Stoicheff

Department of Physics, University of Toronto, Toronto, Ontario, Canada

(Received 4 June 1971)

Single crystals of xenon were grown and Brillouin spectra for various crystal orientations were obtained at a temperature of 156 °K. The spectra exhibited one longitudinal component and either one or two transverse components, depending on crystal orientation. From the observed Brillouin frequency shifts, the adiabatic elastic constants for xenon were evaluated. At 156 °K, $c_{11} = 2.98 \pm 0.05$, $c_{12} = 1.90 \pm 0.04$, $c_{44} = 1.48 \pm 0.04$ in units 10^{10} dyn/cm^2 and the elastic anisotropy was found to be 2.74 ± 0.30. These values were compared with calculated values based on recent theories of lattice dynamics. Good agreement was obtained only with calculations that include all-neighbor interactions. It was also observed that the relative intensities of the Brillouin components were strongly dependent on crystal orientation. An analysis of this variation in intensity gave values of the ratios of the elasto-optic constants for xenon.

I. INTRODUCTION

For many years there has been considerable theoretical and experimental interest in the properties of the rare-gas crystals neon, argon, krypton, and xenon.[1] These elements crystallize in face-centered cubic lattices under the influence of van der Waals interatomic forces. The apparent simplicity of the van der Waals interaction makes these crystals attractive as examples of perfect monatomic lattices and many theories of their lattice dynamics have been developed. In part these theories have been tested against available experimental data on the bulk properties of the rare-gas solids.[1,2] Only recently have techniques for growing rare-gas crystals been developed to the state that single crystals a few millimeters in size can be grown.[3] With such crystals, Simmons and co-workers[4] have been able to obtain accurate measurements of the lattice parameter, isothermal compressibility, thermal expansion, and other thermodynamic properties. However, to properly analyze the dynamical properties of a lattice, and thus to probe the interatomic interaction, accurate measurements of the elastic constants are required. In spite of the improved techniques for growing rare-gas crystals, the elastic constants have been difficult to determine experimentally. For this

purpose, measurements of acoustic velocities in specific crystal directions have been made using ultrasonic and neutron scattering techniques. But to date, these methods have achieved only limited sucess.

Ultrasonic techniques have been used by several groups to investigate argon crystals. Moeller and Squire[5] measured longitudinal and transverse ultrasonic velocities in argon samples assumed to be single crystals oriented so that propagation was along the ⟨110⟩ direction. Gsänger et al.[6] derived elastic constants for argon by combining compressibility data with their measurements of longitudinal ultrasonic velocities in argon crystals oriented by neutron scattering. Keeler and Batchelder[7] have used the ultrasonic pulse-echo technique on argon crystals for which the orientation was determined by backscattering of x rays. The numerical results of these three experiments are surprisingly inconsistent and all imply a much lower elastic anisotropy for argon crystals than can be accounted for theoretically.

Neutron scattering experiments have been used to measure the velocity dispersion curves of krypton, [8] neon, [9] and argon[10] and the elastic constants of neon and argon have been calculated from the data. However, elastic constants derived from the long-wavelength limit of dispersion curves obtained by neutron scattering may differ significantly from adiabatic or isothermal values. [11] The major difficulty with both ultrasonic and neutron scattering techniques is that they require large single crystals (~ 1 cm³) and these are difficult to grow and maintain.

Elastic constants of transparent solids can also be determined by Brillouin spectroscopy as shown by Krishnan[12] and others. Recently, the capabilities of high-resolution Brillouin spectroscopy have been greatly advanced with the development in lasers, interferometers, and detectors so that values of adiabatic elastic constants can be obtained with high precision. For example, values of the elastic constants of the alkali halide crystals KCl, RbCl, KI, [13] and LiF[14] determined from Brillouin spectra are in very good agreement with ultrasonic values. For such crystals, which are stable and easy to manipulate, ultrasonic techniques are simpler and more accurate, but for the rare-gas crystals Brillouin scattering has two distinct advantages. First, it requires only very small samples (~1 mm³) which are relatively easy to grow; and second, unlike ultrasonic measurements, light-scattering studies do not require a transducer or other instrument to be physically bonded to the crystal. Consequently, relatively simple cell geometries can be used which are advantageous to the growth of good single crystals.

In a previous communication[15] we reported on the Brillouin spectrum of xenon single crystals and the first determination of the elastic constants of xenon. The purpose of the present paper is to describe these results and the experimental technique in greater detail. A brief account of the theory of light scattering from acoustic phonons in cubic crystals is given. Particular emphasis is placed on determining the elastic constants from the spectra of single crystals of arbitrary, but known, orientation. Two single crystals were grown for the present experiments. The quality of the crystals and their orientations were determined by x-ray diffraction. The observed Brillouin spectra of both crystals contained one longitudinal and two transverse components, as expected for a cubic crystal. Their frequency shifts and relative intensities were found to vary with orientation in excellent agreement with the predictions of the theory, and values of the adiabatic elastic constants at 156 and 151°K were derived from an analysis of these data with an accuracy of 3%. These results are compared with the experimental elastic data on other rare-gas crystals and with current theoretical values. Some conclusions are drawn regarding the appropriateness of further experiments and theoretical calculations.

II. THEORETICAL ANALYSIS

Brillouin scattering from cubic crystals has been analyzed theoretically by Benedek and Fritsch. [13] The following discussion is intended to extend their theory to describe the spectra scattered from a cubic crystal in an arbitrary orientation with respect to the incident light beam. The generalization was necessary because in the present experiment it was not possible to position the xenon crystals in the most favorable orientations. When a field $\vec{E}(\vec{r}, t) = \vec{E}_0 e^{i(\vec{k}_0 \cdot \vec{r} - \omega_0 t)}$ is incident on a crystalline medium, the far-field scattered amplitude at a point $\vec{R}$ is given by

$$\vec{E}'(\vec{q}, t) = -\left(\frac{\omega_0}{c}\right)^2 \frac{(2\pi)^{3/2}}{4\pi R} \sum_\mu e^{i\vec{k} \cdot \vec{R} - \omega_0 t}$$

$$\times \hat{l}_k [\hat{l}_k \times \delta\epsilon^\mu(\vec{q}, t) \cdot \vec{E}_0], \quad (1)$$

where c is the velocity of light, $\hat{l}_k$ is a unit vector in the direction of the scattered wave vector $\vec{k}$, and $\vec{q} = \vec{k}_0 - \vec{k}$. The fluctuations in the dielectric constant have been written in terms of their spatial Fourier components, viz.,

$$\delta\epsilon(\vec{r}, t) = \left(\frac{1}{2\pi}\right)^{3/2} \sum_\mu \int |d\vec{q}| \, \delta\epsilon^\mu(\vec{q}, t) e^{i\vec{q} \cdot \vec{r}}. \quad (2)$$

The index μ denotes the possibility of a number of branches of the dispersion relations connecting the frequency of the dielectric fluctuation $\omega_\mu(\vec{q})$ and the

wave vector $\vec{q}$. For monatomic face-centered cubic crystals only the acoustic branches are important. No optical branches exist because every atom is at a center of symmetry. In the light-scattering regime ($\vec{q} \sim 2 \times 10^5$ cm^{-1}) the acoutic dispersion is given by the relation

$$\omega_\mu(\vec{q}) = v_\mu(\vec{q})\, q, \quad \mu = 1, 2, 3. \tag{3}$$

In this case the index μ, commonly called the polarization index, denotes the possibility of one "longitudinal" and two "transverse" acoustic modes of the medium associated with the wave vector $\vec{q}$.[16] In the scattered spectrum, the Brillouin frequency shift associated with each acoustic mode is given by $\omega_\mu(\vec{q})$ and thus depends on the velocity $v_\mu(\vec{q})$ of each mode and the magnitude of $\vec{q}$. The direction of $\vec{q}$ is perpendicular to the bisector of the scattering angle θ between $\vec{k}$ and $\vec{k}_0$, so that, neglecting the small change in wavelength between the incident and scattered light, its magnitude is given by the Brillouin equation

$$q = 2k_0 \sin \tfrac{1}{2}\theta. \tag{4}$$

In crystals, $\delta\epsilon^\mu(\vec{q}, t)$ must be expressed as a second-rank tensor $\delta\epsilon^\mu_{ij}(\vec{q}, t)$. The tensor elements determine the polarization and magnitude of the fluctuation in the electric displacement vector $\delta D^\mu_i(\vec{q}, t) = \delta\epsilon^\mu_{ij}(q, t) \cdot (E_0)_j$. These quantities govern the intensity and polarization of the scattered field $E'(\vec{q}, t)$ through the double vector product in Eq. (1). The spectrum of scattered radiation is derived from the autocorrelation function for $E'(\vec{q}, t)$:

$$\frac{d\sigma(\vec{q}, \omega')}{d\Omega} = \frac{c}{16\pi^2} R^2 \int_{-\infty}^{\infty} \langle \vec{E}'(\vec{q}, t+\tau) \cdot \vec{E}'^*(\vec{q}, t) \rangle$$

$$\times\, e^{i\omega'\tau} d\tau, \tag{5}$$

where $d\Omega$ is the solid angle accepted by the detector at a distance R from the point of scattering. The brackets $\langle \cdots \rangle$ indicate a time or ensemble average which is itself independent of time. The autocorrelation function of $\vec{E}'(\vec{q}, t)$ is related to the autocorrelation function of $\delta\epsilon^\mu(\vec{q}, t)$ through Eq. (1). This function can be evaluated for any fluctuating variable using the methods of thermodynamic fluctuation theory if the dependence of the dielectric constant on that variable is known.

The Brillouin spectrum of a crystal arises from fluctuations in the strain tensor $x_{kl} = \partial u_k/\partial r_l$, $\vec{u}$ and $\vec{r}$ being the displacement and position vectors, respectively, of an element of the crystal. The relationship between the stress tensor σ_{ij} and the strain tensor is given by Hooke's law:

$$\sigma_{ij} = c_{ijkl} x_{kl}, \tag{6}$$

where c_{ijkl} is the elastic stiffness, a fourth-rank

tensor. Equation (6) represents nine equations involving 81 constants. Fortunately the elimination of body torques and considerations of symmetry in cubic crystals reduce the number of independent values of c_{ijkl} to three. To simplify the notation, the concept of symmetrized strains,

$$e_{ij} = \frac{1}{2}\left(\frac{\partial u_i}{\partial r_j} + \frac{\partial u_j}{\partial r_i}\right) \tag{7}$$

is customarily introduced in conjunction with a matrix notation in which pairs of tensor indices are reduced to a single subscript running from one to 6 according to the scheme $(11) \to 1$, $(22) \to 2$, $(33) \to 3$, $(23, 32) \to 4$, $(31, 13) \to 5$, $(12, 21) \to 6$. In this manner c_{ijkl} is reduced to a 6×6 matrix c_{mn}. The nonzero values of c_{mn} are referred to as the "elastic constants" of the crystal. For cubic crystals the matrix c_{mn} takes the form

$$\begin{pmatrix} c_{11} & c_{12} & c_{12} & 0 & 0 & 0 \\ c_{12} & c_{11} & c_{12} & 0 & 0 & 0 \\ c_{12} & c_{12} & c_{11} & 0 & 0 & 0 \\ 0 & 0 & 0 & c_{44} & 0 & 0 \\ 0 & 0 & 0 & 0 & c_{44} & 0 \\ 0 & 0 & 0 & 0 & 0 & c_{44} \end{pmatrix}. \tag{8}$$

Certain relationships involving the elastic constants can be deduced immediately. For the crystal to be stable under any infinitesimal deformation the strain energy per unit volume given by

$$U = \tfrac{1}{2} c_{mn} e_m e_n \tag{9}$$

must be positive. This places the following restrictions on the magnitude of the elastic constants:

$$c_{44} > 0, \quad c_{11} > |c_{12}|, \quad c_{11} + 2c_{12} > 0. \tag{10}$$

In accordance with these conditions it is possible that $2c_{44} = c_{11} - c_{12}$, in which case the crystal would be elastically isotropic. However, in general a cubic crystal is elastically anisotropic and the degree of anisotropy is expressed by

$$A = 2c_{44}/(c_{11} - c_{12}). \tag{11}$$

For $A > 1$ the elastic stiffness (Young's modulus) is a maximum in the [111] direction and a minimum in the [100] direction. The converse is true if $A < 1$.

The elastic constants of a crystal are directly related to its compressibility. For a cubic crystal under zero pressure the bulk modulus (the reciprocal of the volume compressibility) is given by

$$B = -V\left(\frac{\partial P}{\partial V}\right) = \tfrac{1}{3}(c_{11} + 2c_{12}). \tag{12}$$

The importance of this relationship is that it provides a means of comparing compressibility mea-

surements for a cubic crystal with independent determinations of the elastic constants. Of course, care must be taken to distinguish between isothermal and adiabatic values of the quantities involved.

An analysis of elastic wave propagation in crystals begins with the equation of motion[17]

$$\rho \, \ddot{u}_i = \frac{\partial \sigma_{ij}}{\partial r_j} \ . \tag{13}$$

If the heat exchanged between volume elements during a period of oscillatory motion is negligible, any part of the medium is thermally isolated and the deformation is adiabatic. In the r_1 direction one obtains from Eqs. (6) and (13)

$$\rho \ddot{u}_1 = c_{11} \, \frac{\partial^2 u_1}{\partial r_1^2} + c_{44} \left(\frac{\partial^2 u_1}{\partial r_2^2} + \frac{\partial^2 u_1}{\partial r_3^2} \right)$$

$$+ (c_{12} + c_{44}) \left(\frac{\partial^2 u_2}{\partial r_1 \partial r_2} + \frac{\partial^2 u_3}{\partial r_1 \partial r_3} \right). \tag{14}$$

Similar equations exist for $\rho \ddot{u}_2$ and $\rho \ddot{u}_3$. For a monochromatic plane-wave solution of the form $u_j = u_{0j} \, e^{i(\vec{q} \cdot \vec{r} - \omega t)}$, this system of equations can be written in the form

$$(\lambda_{ij} - \rho \omega^2 \, \delta_{ij}) \, u_{0j} = 0 \ ,$$

with

$$\lambda_{ij} = (c_{11} - c_{44}) \, q_i^2 + c_{44} \, q^2, \quad i = j$$

$$= (c_{12} + c_{44}) \, q_i q_j \ , \qquad i \neq j \ . \tag{15}$$

The secular equation

$$\left| \lambda_{ij} - \rho \omega^2 \, \delta_{ij} \right| = 0 \tag{16}$$

is cubic in ω^2, resulting in three solutions, $\omega = \pm \omega_\mu(\vec{q})$, with $\mu = 1, 2, 3$, associated with wave vector $\vec{q}$. The polarization of each acoustic mode μ, designated $\vec{\pi}^\mu(\vec{q})$, can be determine by solving Eqs. (15) for u_{0j} on substitution of the respective $\omega = \omega_\mu \times (\vec{q})$. In the particular cases where $\vec{q}$ lies along a direction of high symmetry, for example, $\langle 100 \rangle$, $\langle 111 \rangle$, or $\langle 110 \rangle$, in a cubic crystal the polarization of one mode, $\vec{\pi}^1(\vec{q})$, say, is strictly longitudinal (parallel to $\vec{q}$), while the remaining two modes are strictly transverse [that is, $\vec{\pi}^2(\vec{q})$ and $\vec{\pi}^3(\vec{q})$ are perpendicular to $\vec{q}$]. In two of these directions, $\langle 100 \rangle$ and $\langle 111 \rangle$, the transverse-mode frequencies are degenerate.[17] However, in general, for an arbitrary direction in the crystal, all three modes are nondegenerate in frequency and the polarizations are neither strictly longitudinal nor strictly transverse unless the crystal is elastically isotropic.

The coupling of the elastic waves in a crystal to the dielectric tensor is through the elasto-optic (Pockel's) coefficients p_{ijkl} according to the equation[18]

$$- \frac{\delta \epsilon_{ij}(\vec{r}, t)}{\epsilon_0^2} = p_{ijkl} \, e_{kl}(\vec{r}, t) \ , \tag{17}$$

where ϵ_0 is the permittivity relative to vacuum and $e_{kl}(\vec{r}, t)$ is the symmetrized strain tensor of Eq. (7). The elasto-optic tensor of a cubic crystal, like the elastic stiffness tensor, can be written in the 6×6 matrix notation such that there are only three independent coefficients p_{11}, p_{12}, and p_{44}. From the Fourier transform of Eq. (17) one obtains for the fluctuation of the electric displacement in the crystal

$$\delta \vec{D}^\mu (\vec{q}, t) = \delta \epsilon(\vec{q}, t) \cdot \vec{E}_0$$

$$= (\epsilon_0^2/i) q \, E_0 \, u^\mu(\vec{q}, t) \, \vec{\xi}^\mu, \tag{18}$$

where

$$\xi_i^\mu = \frac{1}{2} p_{44} \left[(\hat{l}_q \cdot \hat{l}_{E_0}) \, (\hat{\Pi}^\mu)_i + (\hat{\Pi}^\mu \cdot \hat{l}_{E_0})(\hat{l}_q)_i \right]$$

$$+ (p_{11} - p_{12} - p_{44})(\hat{\Pi}^\mu)_i (\hat{l}_q)_i (\hat{l}_{E_0})_i$$

$$+ p_{12} (\hat{\Pi}^\mu \cdot \hat{l}_q)(\hat{l}_{E_0})_i \ . \tag{19}$$

The substitutions $\vec{q} = q \hat{l}_q$ and $\vec{E}_0 = E_0 \hat{l}_{E_0}$ have been introduced and $\hat{\Pi}^\mu$ is the unit polarization vector in the direction of the displacement $\vec{u}^\mu(\vec{q}, t)$. The direction and magnitude of $\vec{\xi}^\mu$, $(0 < |\vec{\xi}^\mu| < 1)$ are determined by the relative directions of $\vec{q}$, $\vec{E}_0$, and $\hat{\Pi}^\mu$, and the magnitude of the elasto-optic coefficients. It can be seen from Eq. (1) that in light scattering one measures not $\vec{\xi}^\mu$ but the projection of $\vec{\xi}^\mu$ in the plane perpendicular to the scattered wave vector $\vec{k}$ given by

$$\vec{\xi}^\mu = \hat{l}_k \times (\hat{l}_k \times \vec{\xi}^\mu) \ . \tag{20}$$

The vector $\vec{\xi}^\mu$ therefore determines explicitly the polarization of the radiation scattered from each acoustic mode.

The intensity distribution in the Brillouin spectrum is governed by the autocorrelation function of $\vec{u}^\mu (\vec{q}, t)$. In keeping with the assumption of plane-wave solutions for the dynamics of the crystal, this may be written

$$\langle u^\mu (\vec{q}, t + \tau) \cdot u^{\mu *} (\vec{q}, t) \rangle$$

$$= \left(\frac{V}{(2\pi)^3} \frac{kT}{2\rho \, \omega_\mu (q)^2} \right) e^{\pm i \omega_\mu(\vec{q}) t} - \Gamma_\mu(\vec{q}) |\tau| \ , \tag{21}$$

where the factor in large parentheses is the mean-square amplitude of the fluctuations derived from the equipartition of energy for harmonic oscillators.[13] Finally, the scattering cross section obtained from Eqs. (1), (5), and (18)–(21) is

$$\frac{d\sigma(\vec{q}, \omega')}{d\Omega} = \frac{c}{8\pi} E_0^2 \left(\frac{\omega_0}{c} \right)^4 \frac{V}{(4\pi)^2} \frac{\epsilon_0^4 kT}{2\rho}$$

$$\times \sum_{\mu} \frac{|\vec{\xi}^{\mu}|^2}{\omega_{\mu}(q)^2} \, q^2 \, \frac{1}{\pi} \left(\frac{\Gamma_{\mu}(\vec{q})}{[\omega' - \omega_0 - \omega_{\mu}(\vec{q})]^2 + \Gamma_{\mu}(\vec{q})^2} \right.$$

$$\left. + \frac{\Gamma_{\mu}(\vec{q})}{[\omega' - \omega_0 + \omega_{\mu}(\vec{q})]^2 + \Gamma_{\mu}(\vec{q})^2} \right). \quad (22)$$

The spectrum is seen to consist of three doublets with frequency shifts of $\pm \omega_{\mu}(\vec{q})$, $\mu = 1$, 2, 3. The components are Lorentzian with full widths at half-maximum intensity of $2\Gamma_{\mu}(\vec{q})$. From Eq. (22) it can be seen that the intensity ratio in the Brillouin doublets for two acoustic modes $\mu = a$ and $\mu = b$ is given by

$$\frac{I_a}{I_b} = \left(\frac{\omega_b(\vec{q}) \, |\vec{\xi}^a|}{\omega_a(\vec{q}) \, |\vec{\xi}^b|} \right)^2 . \quad (23)$$

It is well known that the complete spectrum also possesses a central component due to scattering from isobaric entropy fluctuations, but this portion of the spectrum is not of interest in the present experiment and so has been omitted from this discussion.

The objective in the present experiment was to determine the elastic constants of xenon, a face-centered cubic crystal, from experimentally measured Brillouin frequency shifts. In a Brillouin-scattering experiment the wave vector $\vec{q} = \vec{k} - \vec{k}_0$ is defined in space by the scattering configuration. If the crystal orientation is known with respect to the scattering configuration, $\vec{q}$ can be determined relative to the crystal axes. Then Eq. (16) provides a relationship between the elastic constants c_{11}, c_{12}, and c_{44} and the three mode frequencies $\omega_{\mu}(\vec{q})$. It should be noted that, given a set of elastic constants, Eq. (16) can be solved directly for the mode frequencies, but the reverse solution is not straightforward. That is, given three experimentally determined mode frequencies associated with a known wave vector $\vec{q}$ in the crystal, Eqs. (16) cannot be solved directly to obtain the elastic constants. Neighbours and Smith[19] have proposed a method for such a solution based on successive approximations, but this technique is useful only if the elastic anisotropy of the crystal is small. Their method was found to be unsatisfactory for the present analysis. Alternatively, the elastic constants can be obtained by substituting trial values in the dynamical equations and finding the solution which best fits the experimental mode frequencies. This approach is easily carried out when the calculations can be done by computer. The system of equations (15) is a 3×3 eigenvalue problem easily solved by the technique known as Jacobi's method.[20] This technique determines the orthogonal transformation that diagonalizes the matrix $\{\lambda_{ij}\}$. The diagonal elements so obtained (the eigenvalues) yield $\omega_{\mu}(\vec{q})$, $\mu = 1$, 2, 3, and the columns of the transformation matrix (the eigenfunctions) are the unit polarization vectors $\hat{n}_{\mu}(\vec{q})$.

III. EXPERIMENTAL APPARATUS AND TECHNIQUE

A schematic diagram of the complete experiment is shown in Fig. 1. Xenon crystals were grown in a cryostat designed for light-scattering and x-ray diffraction studies. Once a crystal was grown, a Laue diffraction photograph was taken to check that it was single and to determine its orientation. Radiation from a single-frequency laser was incident along the vertical axis of the crystal and Brillouin scattering at an angle of 90° was analyzed with a pressure-scanned Fabry-Perot spectrometer. A detailed description of the apparatus and experimental technique is given below under three headings: (A) cryostat and growth of single crystals, (B) x-ray diffraction and crystal orientation, and (C) Brillouin-scattering technique.

A. Cryostat and Growth of Single Crystals

The cryostat shown in Fig. 1 was constructed of stainless steel and consisted of a 5-liter reservoir for liquid nitrogen connected to a "cold finger" extending into the tail section to provide cooling of the sample cell. The tail section of the cryostat, shown in detail in Fig. 2, was enclosed by a Pyrex envelope 5 cm in diameter which could be removed for easy access to the sample region. Two special windows were incorporated in this envelope: an optical-quality flat window in the bottom for the incident light beam and a thin Mylar window in the back for the incident x-ray beam. The scattered light and diffracted x-rays were transmitted through the curved glass wall of the envelope. Where possible, aluminum foil (not shown in the figures) was attached to the inside of the envelope to reduce the radiant heat transfer to the sample.

The sample cell was constructed from a 2.5-cm length of quartz capillary tubing having a 1.0-mm bore and a wall thickness of ~1 mm. Such a small diameter was found to be necessary since small single crystals are more easily grown and since xenon is such a strong absorber of x-rays that useful Laue photographs in transmission could not be obtained with crystals thicker than 1 mm. A good-quality optical window was constructed for the bottom of the cell by polishing the upper end of a quartz plug (1.0 mm in diameter), fusing it into the bottom of the capillary, and finally polishing the bottom of the cell. As shown in Fig. 2, the sample cell was held and cooled (through thermal conduction) by two phosphor-bronze clips attached to the cold finger. For good thermal contact with the quartz cell two thin rings of aluminum foil (~0.5 cm wide) were cemented to the cell immediately under the clips. One of the clips was attached around the bottom window and the other approxi-
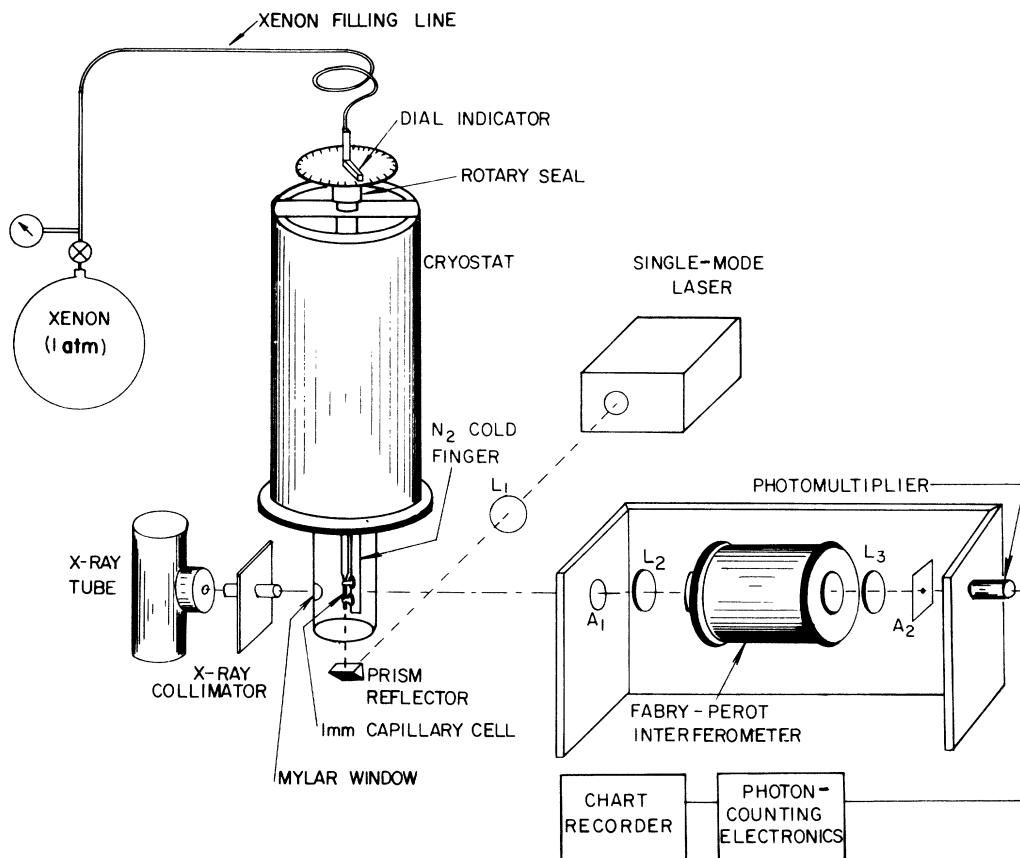
FIG. 1. Experimental arrangement for Brillouin scattering and x-ray diffraction analysis of xenon single crystals.

mately 1 cm higher, providing a clear viewing region ~ 0.7 cm long. The sample cell was attached to a long quartz tube suspended from a rotatable shaft at the top of the cryostat. This shaft also served as a filling line and was attached to a glass flask containing xenon at 1-atm pressure. A heating coil was wrapped around the filling tube to prevent xenon gas from condensing before entering the cell. A calibrated dial mounted at the top of the cryostat was used for rotating the sample cell through a given angle about the vertical axis.

A small heater and thermocouple were mounted on each clip so that the temperature could be controlled and measured at the top and bottom of the sample cell. Temperature control was achieved by balancing the voltage of the lower thermocouple against an adjustable constant voltage supply. A difference voltage was applied to a galvanometer which, when deflected due to a drop in cell temperature, switched on a current source to both heaters. The ratio of the current supplied to the two heaters could be set to produce a temperature gradient of several degrees up the cell. The temperature of the sample could not be measured

directly without seriously affecting the temperature gradient in the sample. However, a calibration of the temperature difference between the sample and the two clips made at the freezing point by observing the position of the xenon solid-liquid interface as the crystal was growing showed that the temperature at the center of the sample was 1.2 °K higher than the average temperature of the two clips. With the correction, temperatures in the vicinity of the freezing point of zenon could be determined to well within ± 1 °K.

At a pressure of 1 atm, xenon liquifies at 165.1 °K and solidifies at 161.4 °K. Initially the temperature of the cell was stabilized at 162 °K and xenon gas was allowed to enter until the cell was full of liquid. Single crystals were grown from the liquid by the following technique. A temperature gradient of approximately 3 °K was established along the cell by adjusting the current ratio through the heaters. The bottom of the cell was then slowly cooled until a tiny "seed" crystal was formed. After annealing the "seed" crystal for several hours, the temperature was slowly decreased (about 1 °K per hour) while maintaining a
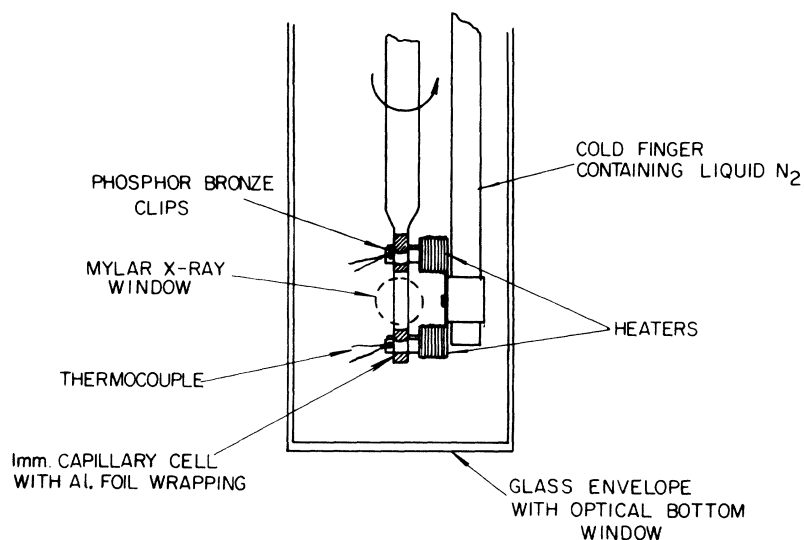
FIG. 2. Cryostat tail section showing the design and mounting of the capillary sample cell as viewed from the Fabry-Perot spectrometer.

fixed temperature gradient until the crystal almost filled the cell. A thin layer of liquid was maintained above the crystal to minimize scattering from the upper surface to the sample. Also, each crystal was grown carefully right from the bottom of the cell to minimize diffuse scattering of the incident laser beam at the window. A dark background in the line of sight of the spectrometer was provided by painting the back wall of the cell with flat-black paint and this helped to reduce the stray light considerably.

B. X-Ray Diffraction and Crystal Orientation

The x-ray source was an oil-cooled tube with a tungsten target. It was operated at 70 kV and 10 mA, and emitted a continuous spectrum of x rays with a low-wavelength cutoff at 0.18 Å. The x-ray beam was collimated and directed at the sample through the Mylar window in the cryostat tail section. To ensure that the x-ray diffraction analysis included the portion of the crystal to be examined by light scattering, the x-ray collimator was carefully aligned with the axis of the Fabry-Perot spectrometer using a laser beam. The cross section of the x-ray beam was ~2 mm in diameter at the sample so that the volume exposed was larger than the volume of crystal contributing to the scattered-light spectrum. The xenon absorption is so high that only the shortest wavelengths emitted by the tube are sufficiently penetrating to produce a good diffraction pattern. The Pyrex and quartz walls of the cryostat and cell are transparent to these short-wavelength x rays but produce a considerable amount of diffuse low-angle scattering that tends to overexpose the central region of the diffraction photograph. This scattering was largely eliminated by positioning a small

lead disk ~5 mm in diameter and 0.6 mm thick in the path of the x-ray beam and in contact with the Pyrex surface. Some of the undiffracted x-ray radiation was still transmitted to indicate the center of the diffraction pattern. The disk was mounted on a vertical needle which also cast a shadow on the diffraction pattern and served as a vertical reference. The photographic film (Ilford type-G x-ray) was mounted 5.0 cm from the sample. A typical diffraction photograph of a single xenon crystal exposed for 1 h is shown in Fig. 3. The silhouettes of the lead disk in the center and its vertical needle mounting are quite evident. A strong vertical absorption line is seen in the undiffracted beam caused by the low transmission through the thickest portion of the cylindrical shaped crystal. This absorption is also evident in each of the diffracted spots and serves as a good indication that the sample is a single crystal since the same diffraction pattern is produced by both sides of the sample. The growth of multiple crystals in the sample cell was easily detectable by the appearance of a large number of small spots in the diffraction photographs.

Usually, the crystal orientation may be easily determined if the diffraction picture exhibits an elliptical pattern of spots that can be identified as a crystal zone (a group of planes containing a common axis). In the present experiment, zone patterns were only seldom observed because of the limited number of diffracted spots and the standard projection techniques of x-ray crystallography could not be used reliably. Instead, a computer program was devised which calculated and plotted on the IBM 7094 Calcomp plotter the diffraction pattern (at 5.0 cm from the sample) for any crystal orientation. By generating diffraction patterns in this way to cover the full range of crystal orientations, it was

θ = 26.0°

ϕ = 239.0°

X = 123.0°

FIG. 3. Laue diffraction photograph of a xenon single crystal taken at a distance of 5.00 cm. Below it (on the same scale) is the computed diffraction pattern that identified the orientation as (26°, 239°, 123°). The solid dots correspond to those actually observed on the photograph.

possible to identify the actual orientation by matching the experimental Laue photograph. A check of each identification was also made by comparing the relative intensities of diffraction spots, estimated from the photographs, with calculated values. The orientation was specified by three Euler angles[21] (θ, ϕ, χ) with the angle corresponding to rotation about the vertical axis in the laboratory reference frame (Fig. 4). In Fig. 3 the Calcomp-plotted diffraction pattern for $(\theta, \phi, \chi) = (26°, 239°, 123°)$ that identified the accompanying Laue photograph has been reproduced. Because the reproduction is not as distinct as the original photograph, the diffraction spots that were actually observed are indicated by solid dots. Each spot is labeled with the Miller indices of the corresponding crystal lattice plane.

Once a crystal orientation was identified, the orthogonal transformation implied by the Euler angles (θ, ϕ, χ) could be used to relate any direction in the laboratory frame (X, Y, Z) to the crystal axis frame (X', Y', Z') as depicted in Fig. 4. In particular, it was possible to determine the direction of the phonon wave vector $\vec{q}$ and the polarization of the incident radiation field $\vec{E}_0$ in the crystal.

C. Brillouin-Scattering Technique

The He-Ne laser used in this experiment operated on a single longitudinal cavity mode stabilized to the Lamb dip in the Doppler-broadened gain profile of the neon emission. The output power was approximately 0.4 mW in the fundamental (TEM_{00}) transverse mode. The beam was focused in the sample cell with a 25-cm focal-length lens $(L_1$ in Fig. 1). The ability to focus this TEM_{00} beam to a diameter of approximately 0.2 mm made the use of extremely small samples feasible.

FIG. 4. Euler angles relating the crystal reference frame (X', Y', Z') and the laboratory reference frame (X, Y, Z). The directions of $\vec{k}_0$, $\vec{k}$, and $\vec{q}$ defined by scattering configuration are shown.

The Fabry-Perot spectrometer is shown in Fig. 1. It consists of a collection lens (L_2), the Fabry-Perot interferometer, a second lens (L_3), which focuses the interference pattern on a screen with a pinhole aperture (A_2), and a photomultiplier tube. A short-focal-length lens not shown in the figure refocuses light from the pinhole onto the photocathode of the tube. Aperture A_1 in front of the spectrometer serves to limit the solid angle of the scattered light that is collected. The Fabry-Perot interferometer consisted of two 1.5-in.-diam plates flat to $\lambda/200$ and dielectrically coated to a reflectivity of 98% at 6328 Å. They were separated by an Invar etalon 0.9993 cm long so that the spectral free range of the instrument was 15 000 Mc/sec. The interferometer was mounted in a metal chamber with windows in either end. Pressure scanning was accomplished by evacuating this chamber and allowing air to reenter through a needle valve and flow-rate controller

An instrumental finesse of 100 was achieved with this interferometer. Good sensitivity was obtained along with this high resolving power by carefully choosing the components of the system. The optimum arrangement exists when the radius R of the aperture A_2 in the focal plane of L_3 equals the spatial extent $\Delta\nu_R$, the full width at half-intensity of the central interferometer fringe. For a small angle θ from the optic axis, the spatial dispersion derived from the Fabry-Perot equation is given by

$$dl/d\nu = f^2/l\nu ,$$

where f is the focal length of L_3 and $l = \theta f$. Upon integrating, with $\nu_0 \leq \nu \leq \nu_0 + \Delta\nu_R$, $0 \leq l \leq R$, one obtains

$$\Delta\nu_R/\nu_0 = R^2/2f^2 .$$

For the 1-cm etalon used in the present experiment, $\Delta\nu_R \sim 100$ Mc/sec, and for a 56.0-cm focal-length lens (L_3), the optimum diameter of the aperture A_2 by this criterion is 0.7 mm. In the present experiment a slightly smaller aperture was used for better resolution. Finally, the lens L_2 was chosen to have a focal length of 30.0 cm so that the image of the beam in the sample, estimated to be 0.2 mm in diameter, was magnified to approximately the size of the aperture. This means that only scattering which occurred in a volume of the sample with dimensions ~ 0.25 mm was detected by the spectrometer. Thus, if the x-ray diffraction indicated a single crystal with dimensions ~ 1 mm, there could be no doubt that the scattered spectrum originated from that crystal.

The light intensity passing through aperture A_2 was measured by an ITT FW-130 photomultiplier tube and "photon-counting" electronics consisting of a preamplifier, amplifier, pulse-height analyzer, and linear ratemeter. By cooling the tube to $-20\,°C$ in a Peltier-effect chamber, the dark count-

ing rate was reduced to ~ 1 per second. Brillouin spectra were recorded on a strip-chart recorder which ran at a constant speed. A 10-sec integrating-time constant was used and the scanning rate was 1 h per spectral free range.

IV. EXPERIMENTAL RESULTS

Two single crystals of xenon were grown for this investigation: Crystal 1 was studied at 156 °K and crystal 2 at 156 and 151 °K. X-ray diffraction photographs showed the crystals to be single and at least 2 mm in length and 1 mm in diameter. The two crystals grew in slightly different orientations with respect to the cell axis and for neither crystal was a principal symmetry axis aligned with the cell axis.

A. Brillouin Spectra

The Brillouin spectrum of crystal 1 was recorded for eight different orientations, with the angle θ changed in increments of 10° by rotating the sample cell about its vertical axis. The incident laser light was polarized perpendicular to the scattering plane and the spectrometer measured the total scattered intensity at 90° (I_V^{tot}). (Attempts to observe depolarized scattering, that is, scattered intensity in
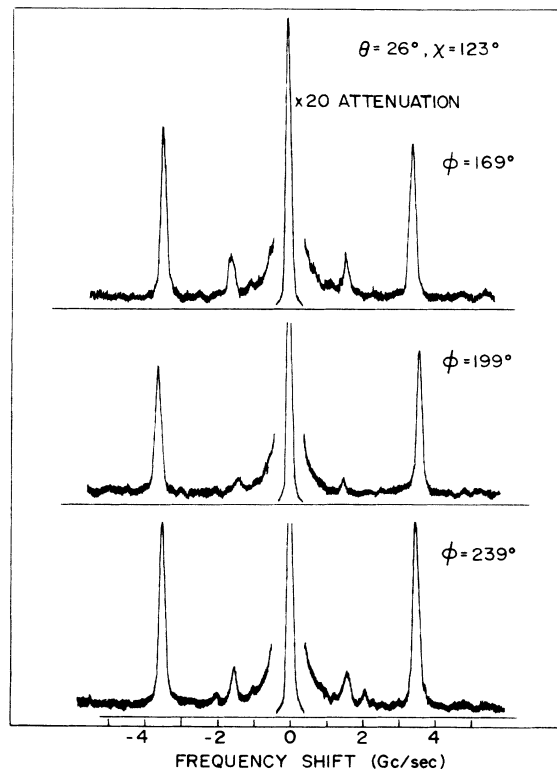
FIG. 5. Brillouin spectra of xenon crystal 1 in three different orientations specified by the Euler angles (θ, ϕ, χ).

TABLE I. Experimental frequency shifts (in Gc/sec) of longitudinal and transverse Brillouin components as a function of crystal orientation.

	Angle ϕ (deg)	L	T_1	T_2
Crystal 1	169	3.463 ± 0.002[a]	$\cdots$	1.583 ± 0.001[a]
$T = 156\,°K$, $P = 1$ atm,	179	3.517 ± 0.001	$\cdots$	1.493 ± 0.002
$\theta = 26°$, $\chi = 123°$	189	3.545 ± 0.005	$\cdots$	1.383 ± 0.012
	199	3.555 ± 0.004	$\cdots$	1.426 ± 0.003
	209	3.530 ± 0.002	$\cdots$	1.488 ± 0.001
	219	3.492 ± 0.003	$\cdots$	1.552 ± 0.003
	229	3.454 ± 0.008	1.959 ± 0.006	1.568 ± 0.002
	239	3.415 ± 0.002	2.027 ± 0.011	1.515 ± 0.004
Crystal 2	283	3.451 ± 0.003	$\cdots$	1.555 ± 0.009
$T = 156\,°K$, $P = 1$ atm,	298	3.493 ± 0.003	$\cdots$	1.449 ± 0.013
$\theta = 70°$, $\chi = 108°$	318	3.484 ± 0.003	$\cdots$	1.443 ± 0.004
	338	3.427 ± 0.003	$\cdots$	1.621 ± 0.003
	343	3.396 ± 0.003	$\cdots$	1.647 ± 0.003
	348	3.387 ± 0.003	1.996 ± 0.025	1.668 ± 0.010
$T = 151\,°K$, $P = 1$ atm,	348	3.426 ± 0.023	2.055 ± 0.015	1.708 ± 0.018
$\theta = 70°$, $\chi = 108°$				

[a]Average deviation of the measured values.

the scattering plane, or I_V^H, were unsuccessful with the available sensitivity.) Brillouin spectra observed for three crystal orientations are shown in Fig. 5. The central component is the most intense feature and results from the unavoidable stray scattering from the small sample cell. However, because of the high resolution of the Fabry-Perot spectrometer this did not seriously affect the Brillouin components. It is evident from these spectra that the frequency shifts of the Brillouin components vary significantly with orientation. More striking is the dramatic change in the relative intensities of the components. In the first spectrum ($\phi = 169°$) only one transverse doublet is observed; in the second ($\phi = 199°$) even that transverse mode is almost undetectable in the background noise of the spectrum. In the bottom spectrum ($\phi = 239°$) all three doublets are observed, although the second transverse component is very weak. Of the eight orientations in which crystal 1 was studied only two spectra revealed all three Brillouin doublets.

Each spectrum was recorded in at least three spectral orders over which the scan rate was linear to better than 1%. The measured Brillouin shifts for each of the eight orientations are summarized in Table I and plotted as a function of the angle ϕ in Fig. 6. (T_1 and T_2 refer to the high- and low-frequency transverse modes, respectively.) Each value is the average of at least six measurements for which the average deviation has been included. Table II lists the intensity ratios of the observed transverse and longitudinal components. These ratios were estimated from the heights of the best line shapes that could be drawn through the noise level of each spectrum and are considered to be approximate values only, because of the low inten-

sities of the transverse components.

The observed Brillouin shifts for six orientations of crystal 2 are summarized in Table I and Fig. 6. The variation in the mode frequencies with crystal orientation is similar to that found for crystal 1 but not identical. The small difference in the shapes of the curves is due to only slight differences in the crystal orientations as both crystals were found to have a $\langle 311 \rangle$ axis almost parallel to the cell axis. The angle between the cell axis and the closest $\langle 311 \rangle$ direction in crystal 1 was $4°$; in crystal 2 it was $2°$. All three Brillouin components were observed for only one orientation of crystal 2, $\phi = 348°$, and this orientation was chosen for a study of the temperature dependence of the spectrum. The temperature was lowered at a rate of less than $1\,°K$ per hour, to $151\,°K$, and the Brillouin spectrum was recorded. Only slight changes in the frequency shifts were observed (Table I). X-ray diffraction revealed that at $151\,°K$ the main crystal was still

TABLE II. Experimental intensity ratios as a function of crystal orientation for crystal 1 ($T = 156\,°K$, $P = 1$ atm) ($\theta = 26°$, $\chi = 123°$).

ϕ (deg)	$I(T_1)/I(L)$	$I(T_2)/I(L)$
169	$\cdots$	0.199 ± 0.018[a]
179	$\cdots$	0.140 ± 0.016
189	$\cdots$	0.048 ± 0.015
199	$\cdots$	0.054 ± 0.010
209	$\cdots$	0.148 ± 0.015
219	$\cdots$	0.173 ± 0.010
229	0.047 ± 0.010	0.158 ± 0.010
239	0.033 ± 0.010	0.140 ± 0.010

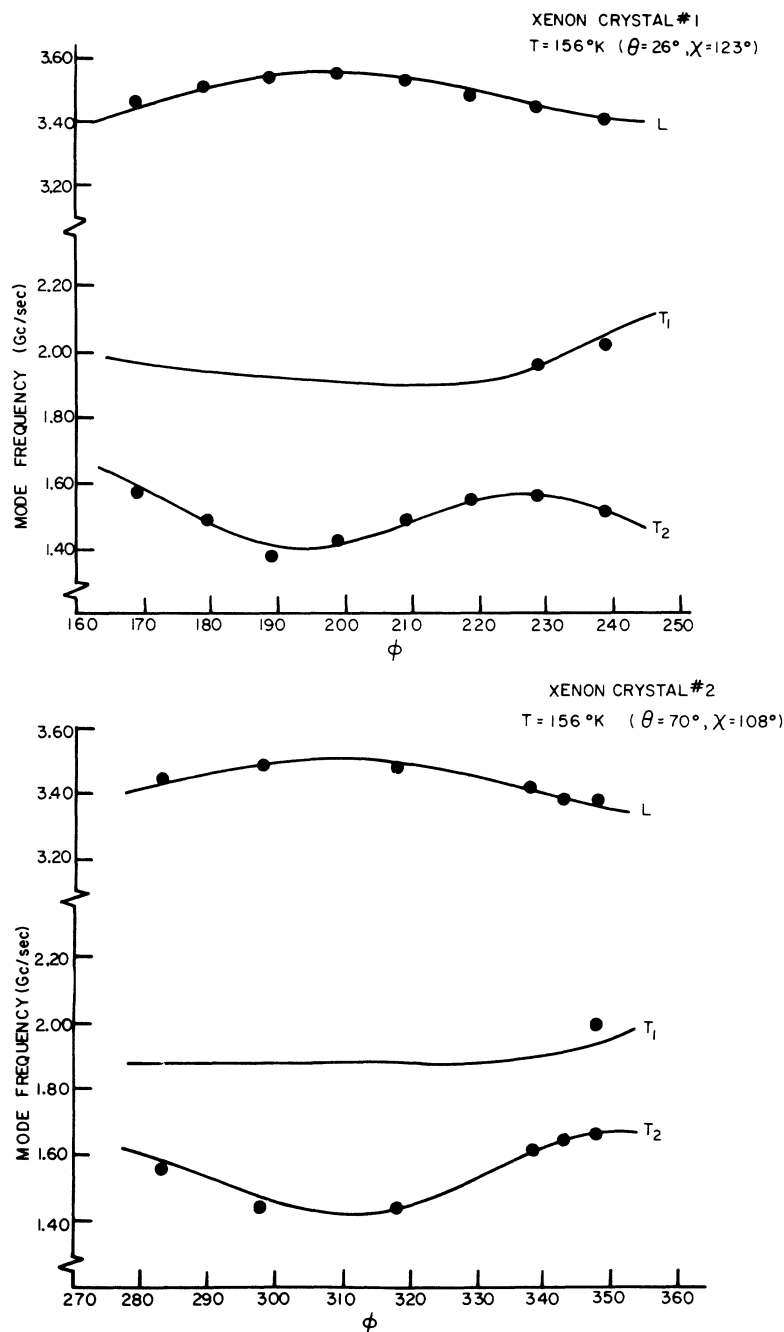[a]Average deviation of the measured values.

FIG. 6. Acoustic-mode frequencies of xenon crystals 1 and 2 as a function of the orientation angle ϕ. The experimental Brillouin shifts are indicated by the solid dots. The curves represent the best theoretical fit to the L and T_2 data.

intact but there was evidence of a few tiny crystallites, probably near the walls of the cell. An attempt was made to cool the crystal an additional 5 °K but visual inspection with the laser beam passing through the sample showed evidence of extensive breakage. At 146 °K cooling was discontinued and the temperature was held constant for 24 h. The sample appeared to anneal at this temperature but x-ray analysis revealed that it consisted of many small crystals of varied orientation.

B. Evaluation of Elastic Constants and Experimental Uncertainty

The elastic constants were determined by finding the solution of the dynamical equations (15) which best fitted the experimental frequency shifts given in Table I. Since most of the spectra exhibited only two Brillouin components, the longitudinal (L) and one transverse (T_2), while three of the spectra exhibited all three components, two methods of analysis were adopted in order to make

the best use of the data. The first analysis was carried out only for those orientations where all three Brillouin frequency shifts were measured, namely, $\phi = 229°$, $239°$ for crystal 1 and $\phi = 348°$ for crystal 2. In this analysis an independent determination of all three elastic constants c_{11}, c_{12}, and c_{44} was made for each orientation from the three frequency shifts. The values of the elastic constants obtained by this method of analysis are given in Table III.

In the second method of analysis, the solutions of the dynamical equations corresponding to the modes L and T_2 were fitted by least squares to the associated frequency shifts for all eight orientations of crystal 1 and all six orientations of crystal 2. The resulting solutions are plotted as functions of the angle ϕ in Fig. 6 and compared with the experimentally measured frequency shifts. The agreement is very good. Also, although the T_1 mode was not fitted in these calculations, good agreement with the observed frequency shifts is seen for those orientations where scattering from this mode was observed. The values of the elastic constants determined in this way are given in Table III and labeled (all ϕ).

In order to properly assess the accuracy with which the elastic constants are determined by Brillouin scattering, two types of uncertainty must be considered: one which affects the absolute magnitude of all three elastic constants in the same way, and another which primarily affects their relative values. Uncertainty in the physical constants of the sample such as its density, refractive index, temperature, and uncertainty in the scattering angle fall into the first category. These quantities occur as common factors in the equation used in deriving the elastic constants from the Brillouin frequency shifts. In the present experiment, the uncertainty in all four factors combined was estimated to be less than ±1%.[22,23] The second type of uncertainty is more important.

The relative values of the elastic constants de-

TABLE III. Adiabatic elastic constants of xenon determined from the Brillouin spectra. Density $\rho = 3.413$ and 3.430 g/cm^3 (Ref. 22) at 156 and 151 °K, respectively, and refractive index $\eta = 1.449$ and 1.451 (Ref. 23).

T (°K)	Elastic constants (10^{10} dyn/cm^2)			Determination
	c_{11}	c_{12}	c_{44}	
156	2.95	1.88	1.49	Crystal 1 ($\phi = 229°$)
	2.97	1.90	1.46	Crystal 1 ($\phi = 239°$)
	2.94	1.89	1.50	Crystal 1 (all ϕ)
156	3.00	1.92	1.47	Crystal 2 ($\phi = 348°$)
	3.07	1.92	1.38	Crystal 2 (all ϕ)
151	3.03	1.90	1.56	Crystal 2 ($\phi = 348°$)

TABLE IV. Deviations in the elastic constants resulting from variations in the Euler angles (θ, ϕ, χ) for crystal 1.

$\Delta\theta$ (deg)	$\Delta\phi$ (deg)	$\Delta\chi$ (deg)	Δc_{11} (%)	Δc_{12} (%)	Δc_{44} (%)
(a) For only two Brillouin shifts					
-2	0	0	-1.3	-1.4	$+0.5$
$+2$	0	0	$+13.3$	$+14.4$	-18.7
0	-2	0	$+0.2$	$+1.0$	-0.7
0	$+2$	0	$+6.1$	-0.2	-0.5
0	0	-2	$+12.3$	$+13.4$	-17.4
0	0	$+2$	$+1.6$	$+2.4$	-2.4
(b) For all three Brillouin shifts					
-2	0	0	-1.7	$+2.5$	$+1.3$
$+2$	0	0	-1.7	$+4.0$	$+2.0$
0	-2	0	-2.3	-1.3	$+2.7$
0	$+2$	0	$+2.3$	$+1.3$	-2.0
0	0	-2	-3.3	-4.5	$+3.3$
0	0	$+2$	$+3.0$	$+4.5$	-2.7

termined by the two methods used in this experiment were very sensitive to inaccuracies in the orientation angles (θ, ϕ, χ) and to inaccuracies in the measured Brillouin shifts. It is impossible to describe this sort of uncertainty analytically because it depends on a number of factors. For instance, the sensitivity to errors in the orientation angles (θ, ϕ, χ) depends not only on the magnitude of the errors, say, $\Delta\theta$, $\Delta\phi$, $\Delta\chi$, but also on the values of the angles θ, ϕ, and χ themselves. For this reason, the best estimate that could be made of the effect of such errors on the elastic constants was

TABLE V. Deviations in the elastic constants resulting from variations in the Brillouin shifts for crystal 1.

(a) For two Brillouin shifts: data analyzed using pairs of orientations instead of all orientations			
Crystal orientations (deg)	Δc_{11} (%)	Δc_{12} (%)	Δc_{44} (%)
$\phi = 169, 239$	$+8.9$	$+9.1$	-13.1
$\phi = 179, 239$	-5.5	-5.3	$+9.7$
$\phi = 189, 239$	-5.5	-2.1	$+6.9$
$\phi = 199, 239$	-5.5	-7.5	$+9.7$
$\phi = 209, 239$	-1.0	-2.1	$+2.1$
$\phi = 219, 239$	0.0	-1.6	$+0.7$
$\phi = 229, 239$	-5.5	-7.5	$+9.7$

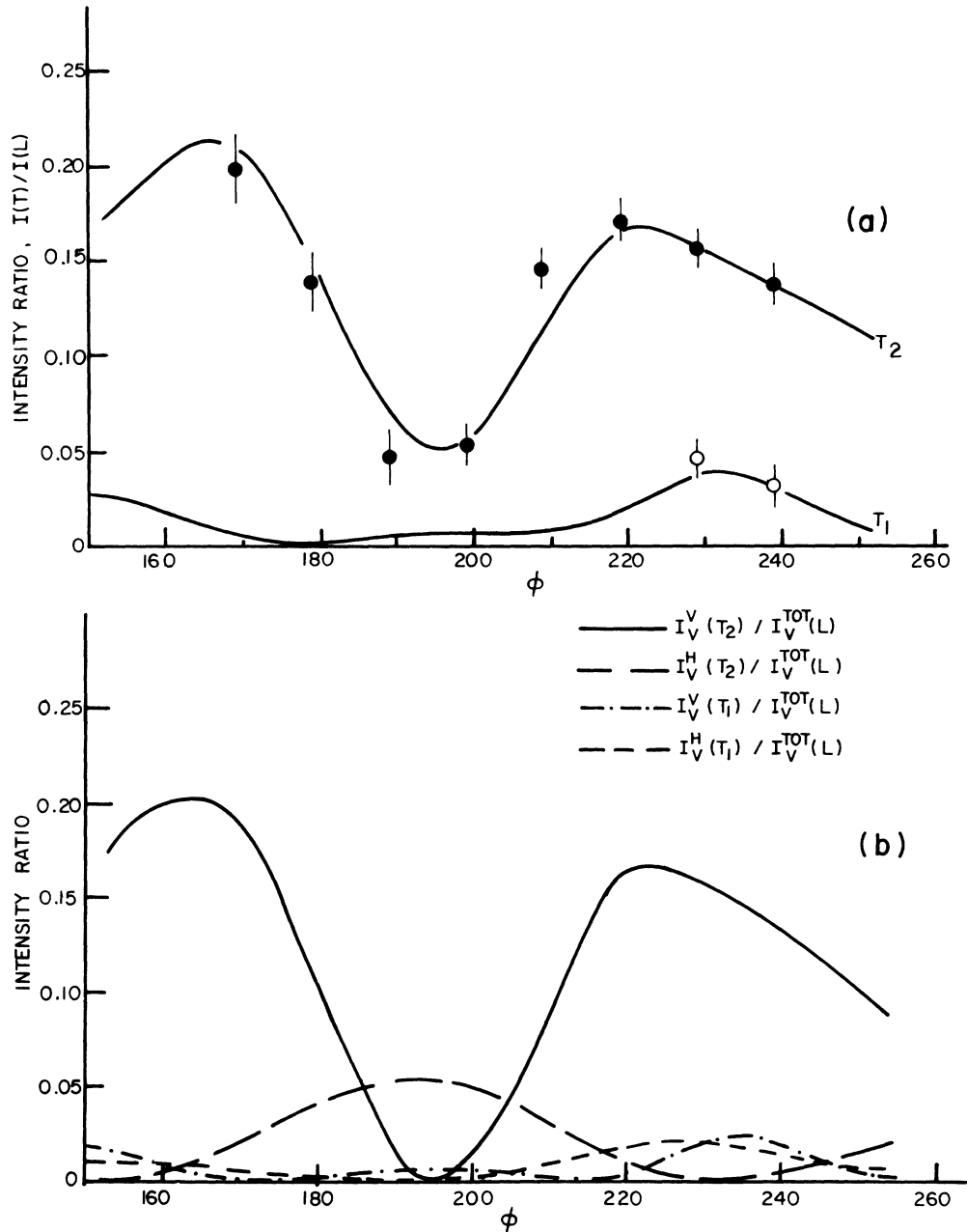| (b) For three Brillouin shifts					
$\Delta\nu$(L) (Gc/sec)	$\Delta\nu$(T$_1$) (Gc/sec)	$\Delta\nu$(T$_2$) (Gc/sec)	Δc_{11} (%)	Δc_{12} (%)	Δc_{44} (%)
-0.02	0	0	-1.7	-2.1	$+0.7$
$+0.02$	0	0	$+1.4$	$+3.2$	0.0
0	-0.02	0	$+1.7$	$+1.6$	-2.0
0	$+0.02$	0	-1.7	-1.6	$+3.4$
0	0	-0.02	-1.0	$+1.1$	$+0.7$
0	0	$+0.02$	$+1.0$	-0.5	0.0

FIG. 7. Intensity ratios of the Brillouin components in the spectrum of crystal 1 as functions of ϕ. (a) The points are experimental ratios from the I_V^{tot} spectra; the curves represent the best theoretical fit. (b) Calculated intensity ratios for 90° scattering polarized perpendicular and parallel to the scattering plane, as a function of the orientation ϕ.

to introduce deliberate errors in the data and observe the change in recalculated values of the elastic constants. The results obtained using the data for crystal 1 are shown in Tables IV and V. The first table shows the effect of altering each of the Euler angles θ, ϕ, and χ by 2°, a value estimated to be the upper limit of the experimental uncertainty in the x-ray diffraction method. When the elastic constants were determined from only two

Brillouin shifts, measured in several crystal orientations, large deviations ($\sim \pm 15\%$) were produced in some cases. However, for the determinations involving all three Brillouin shifts, the same changes in the Euler angles produces much smaller changes ($\sim \pm 3\%$) in the elastic constants. Consequently, the latter method is much less sensitive to small inaccuracies in θ, ϕ, and χ.

Table V indicates the variations in the values of

the elastic constants due to uncertainties in the experimental Brillouin frequency shifts. The uncertainties were assessed in two ways. First, the data for all orientations were analyzed in pairs of crystal orientations using only two Brillouin shifts. In this way the actual uncertainties in the frequency shifts for different orientations were emphasized. Formerly, such uncertainties were minimized by using a least-squares fit over all eight orientations. For this analysis of the data, deviations as large as $\pm 10\%$ in the values of the elastic constants were obtained. Second, changes were made in the data for one orientation (crystal 1, $\phi = 229°$), where all three Brillouin components were observed. The experimental frequency shifts were individually changed by ± 0.02 Gc/sec. The effect on the elastic constants was less than $\pm 3.5\%$ in all cases as shown in Table V.

It is apparent that determining the elastic constants of a cubic crystal by Brillouin scattering can be greatly facilitated when all three Brillouin components can be observed. Not only is it much easier to make measurements for a single orientation rather than having to rotate the crystal, but the experimental accuracy is greatly improved.

In the present experiment, the Euler angles were determined to better than $\pm 2°$ and the Brillouin shifts in most cases could be measured to within ± 0.02 Gc/sec. In view of the above analysis, the excellent agreement between the values of the elastic constants listed in Table III for the two crystals at 156 °K indicates that, in fact, the experimental accuracy was much better than this. To summarize the experimental data, the average values of the adiabatic elastic constants determined for xenon are

$T = 156$ °K:

$c_{11} = 2.98 \pm 0.05, \quad c_{12} = 1.90 \pm 0.04, \quad c_{44} = 1.48 \pm 0.04,$

$T = 151$ °K:

$c_{11} = 3.03 \pm 0.05, \quad c_{12} = 1.90 \pm 0.04, \quad c_{44} = 1.56 \pm 0.04,$

in units of 10^{10} dyn/cm^2. In computing these average values more weight has been given to the values in Table III determined from three Brillouin shifts. The uncertainty in each case was estimated from the variation found in Table III weighted in accordance with the above analysis.

C. Ratios of Elasto-Optic Constants

Finally, the intensity ratios of the spectral components for crystal 1 were used to estimate relative values of the elasto-optic (Pockel's) coefficients for xenon. These values should be representative of the elasto-optic coefficients for all the rare-gas crystals and therefore may be useful in predicting the scattering intensities in future experiments. The intensity

ratios listed in Table II are plotted as a function of orientation in Fig. 7(a). These intensity ratios are a function of crystal orientation, of frequency and polarization of the acoustic modes in the crystal, and of relative magnitudes of the elasto-optic coefficients [see Eqs. (19), (20), and (23)]. By varying the ratios p_{12}/p_{11} and p_{44}/p_{11}, the intensity ratios of the Brillouin components in the I_V^{tot} spectrum were calculated using Eq. (19) and fitted by least squares to the values for the T_2 mode plotted in Fig. 7(a). The best agreement with the experimental intensity ratios was found for

$$p_{12}/p_{11} = 1.45, \quad p_{44}/p_{11} = -0.20 .$$

The fitting was carried out only for the intensity ratio involving the stronger transverse mode (T_2). It is therefore reassuring to note that the theory predicts the strongest intensity for the T_1 component at precisely the orientations for which it was observed.

With these values for the ratios of the elasto-optic coefficients it is possible to predict the relative intensities of scattered light polarized perpendicular or parallel to the scattering plane for any two acoustic modes. In Fig. 7(b) an example of the variation in intensity of scattering from the T_1 and T_2 modes as a function of crystal orientation is shown, in each case separated into the constituent polarizations I_V^V and I_V^H. The intensity ratios are calculated relative to the common denominator I_V^{tot} (L), the total scattered intensity from the longitudinal acoustic mode. The crystal orientation taken is that of the experimental data for crystal 1. It is now apparent why no depolarized Brillouin spectrum was observed for crystal 1. Although not shown in Fig. 7(b), the I_V^H scattering from the L mode is very weak in all orientations. For the transverse acoustic modes, scattering from the T_2 mode is the strongest, but only significantly depolarized in the vicinity of $\phi = 195°$, where it is the weakest (see the spectrum for $\phi = 199°$ in Fig. 5). Where it was observable, the T_1-mode intensity is ~50% depolarized. Consequently, with the added loss in sensitivity (~30%) introduced experimentally by inserting a polaroid analyzer it is not surprising that no depolarized spectrum was observed.

V. DISCUSSION

The present experiment has led to the first determination of the elastic constants of xenon crystals. The values are of the order of those for argon and neon (Table VI) and, typically, one to two orders of magnitude smaller than the elastic constants of cubic crystals such as Cu, Ni, KCl, KI, and LiF. Thus van der Waals solids like the rare-gas crystals are elastically very soft in comparison with metallic and ionic crystals.[17] It is also of interest that for

TABLE VI. Experimental elastic constants and elastic anisotropy for rare-gas crystals.

Experiment	Rare gas	Temp. (°K)	c_{11}	c_{12} (10^{10} dyn/cm²)	c_{44}	A
Light scattering	xenon	156	2.98	1.90	1.48	2.74 ± 0.30
Ultrasonic (Ref. 5)	argon	77	3.07	1.44	0.69	0.85
Ultrasonic (Ref. 6)	argon	77	3.35	1.01	0.93	0.80 ± 0.28
		4	5.29	1.35	1.59	0.81 ± 0.21
Ultrasonic (Ref. 7)	argon	77	2.78	1.43	0.92	1.36 ± 0.22
		4	4.38	1.82	1.63	1.22 ± 0.17
Neutron diffraction (Ref. 10)	argon	4	4.11	1.90	2.10	1.90
Neutron diffraction (Ref. 9)	neon	4.7	1.69	0.97	1.00	2.78 ± 0.38

xenon the elastic anisotropy defined in Eq. (11) has the high value $A = 2.74 \pm 0.30$.

The existing measurements of the elastic constants of other rare-gas crystals have been made using ultrasonic and neutron scattering techniques. Three independent ultrasonic experiments have been reported for argon[5,7] and a summary of elastic constants and anisotropy is included in Table VI. Also listed are neutron scattering measurements of the elastic constants of neon[9] and argon.[10] All three ultrasonic experiments indicate a much smaller elastic anisotropy for argon near its melting point than that for xenon at 156 °K. In fact, for two of the experiments $A < 1$, suggesting an anisotropy opposite in sense to that predicted theoretically for argon.[24] In view of the present results for xenon, it seems more likely that the low anisotropy measured for argon is indicative of some polycrystalline structure in the relatively large samples used for these experiments.

Measurements of the bulk compressibility of xenon crystals are available and these can be used to substantiate the values for two of the elastic constants, c_{11} and c_{12}. Packard and Swenson[22] found for the isothermal bulk modulus the value B_T = $(1.48 \pm 0.2) \times 10^{10}$ dyn/cm². From the present determination of c_{11} and c_{12}, the adiabatic bulk modulus defined by Eq. (12) is B_s = $(2.26 \pm 0.04) \times 10^{10}$ dyn/cm². However, in order to compare the $\cdot$ values, the adiabatic-isothermal correction[25] must be made, namely,

$$c_{11}^{ad} - c_{11}^{iso} = c_{12}^{ad} - c_{11}^{iso} = \gamma^2 \rho C_v T, \quad c_{44}^{ad} - c_{44}^{iso} = 0.$$
$$(24)$$

Here, $\gamma = \beta B_s / \rho C_p$ is the thermodynamic Grüneisen parameter. For xenon at $T = 156$ °K, the density[22] $\rho = 3.413$ g/cm³ at 1-atm pressure, the volume expansivity[26] $\beta = 12.8 \times 10^{-4}/$°K, and the specific heats[26,27] C_p and C_v are 8.2 and 4.9 cal/mol °K, respectively. Together with the adiabatic bulk modulus, these values give $\gamma = 3.23$ for the Grüneisen parameter. The adiabatic-isothermal correction to c_{11} and c_{12} is therefore 0.86×10^{10} dyn/cm² at

156 °K, and the isothermal elastic constants derived from the adiabatic values at 156 °K are $c_{11}^{iso} = 2.12$, $c_{12}^{iso} = 1.04$, and $c_{44}^{iso} = 1.48$ in units of 10^{10} dyn/cm². Thus, the isothermal bulk modulus is $B_T = 1.40 \times 10^{10}$ dyn/cm², in good agreement with the value measured by Packard and Swenson.[22]

A comparison of the experimental elastic constants of xenon with values calculated on the basis of recent theories of lattice dynamics is of primary interest. For temperatures above approximately one-third the triple-point temperature, the elastic properties of the rare-gas crystals are expected to show considerable anharmonicity due to the large (>6%) rms amplitudes of the lattice vibrations. As a result, the Born–von Kármán theory of lattice dynamics is not adequate to describe the properties of these crystals at high temperature and various theories have been devised to extend calculations of the elastic constants beyond the zero-temperature values of Barron and Klein.[28] By using a perturbation expansion of the Helmholtz free energy, Feldman, Klein and Horton,[24] have derived quasiharmonic elastic constants for argon, krypton, and xenon. The results of their calculations for xenon, based on a Lennard-Jones (6-12) potential and restricted to nearest-neighbor interactions (NN), are shown by the solid curves in Fig. 8. These curves terminate at 106 °K because the quasiharmonic approximation (QH) for xenon breaks down at higher temperatures due to the large amplitude of the vibrations. Another approach, known as self-consistent phonon theory[29] (SC), provides a much more adequate treatment of the lattice dynamics of rare-gas crystals over their complete temperature range. Calculations based on this technique generally show much better agreement with the experimental temperature dependence of quantities such as the volume expansivity, heat capacity, and isothermal bulk modulus.[2,30] Klein[31] has calculated the elastic constants for xenon using the lowest-order SC scheme, again for a Lennard-Jones (6-12) potential acting between nearest-neighbors only. His results are shown by the dashed curves in Fig. 8. Since the calculations extend
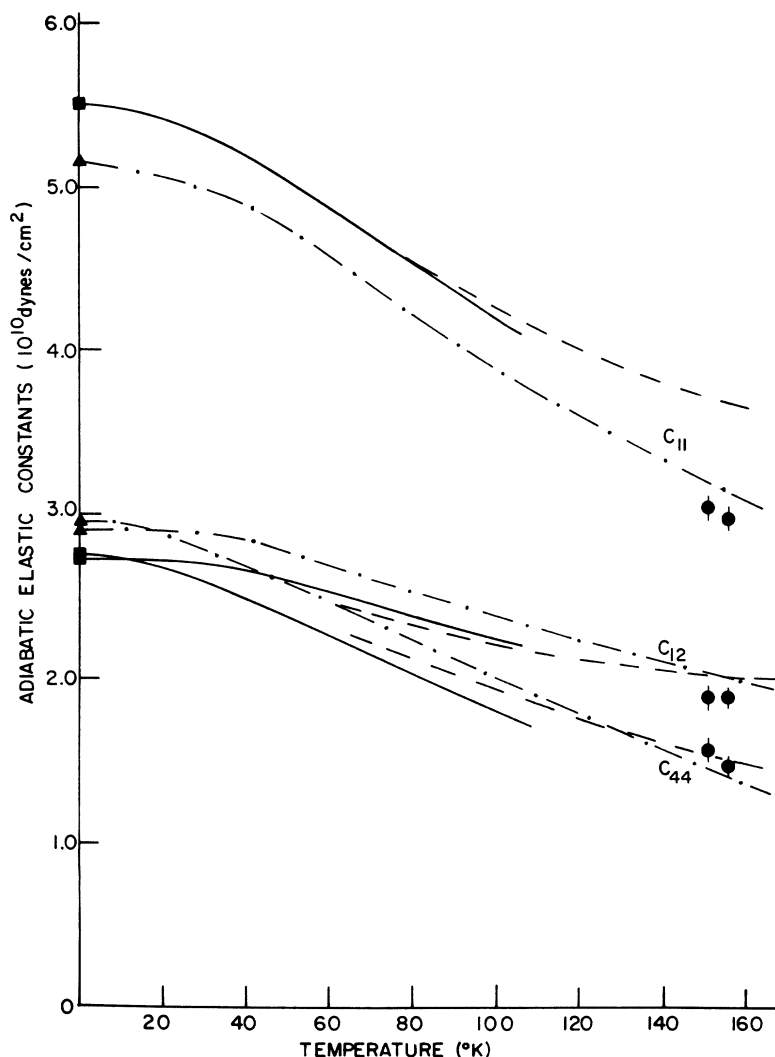
FIG. 8. Temperature dependence of the adiabatic elastic constants. The experimental results are plotted as large solid dots. The solid and dashed curves correspond to the nearest-neighbor quasi-harmonic (Ref. 24) and self-consistent phonon (Ref. 31) calculations, respectively. The dash-dotted curve is obtained from the 107-neighbor quasiharmonic calculation of Ref. 34. The values at 0 °K are those of Barron and Klein listed in Table VII.

to 160 °K, they can be directly compared with the present experimental results. [Klein's calculation actually evaluated the isothermal elastic constants and these have been converted to adiabatic values for presentation in Table VII and Fig. 8 by means of the adiabatic-isothermal correction given by Eqs. (24).] The value of c_{11} obtained from the SC theory is much higher than observed experimentally in spite of the good agreement obtained for c_{12} and c_{44}.

The SC theory used by Klein did not include odd derivatives of the interatomic potential. Although this first-order SC theory is not completely adequate for calculating the volume expansivity and heat capacity, such calculations of the isothermal bulk modulus show good agreement with measured values.[30] The "improved self-consistent" scheme (ISC), which inculdes odd derivatives of the potential and works much better for the former quantities,

produces only a slightly lower value of the bulk modulus for argon near the melting point.[30] For xenon, Klein[31,32] calculates a similar decrease in B_T of less than 4% at 160 °K. It is unlikely, therefore, that the discrepancy in c_{11} can be accounted for by the more elaborate ISC calculations.

Recently, Monte Carlo computer experiments have been used to simulate the dynamical behavior of rare-gas crystals. Calculations for argon[33] have been carried out using 108 particles interacting with a Lennard-Jones (6-12) potential. Holt et al.[34] have subsequently shown that the adiabatic elastic constants derived from quasiharmonic lattice-dynamics calculations including 107-particle interactions agree very well with the Monte Carlo results for argon. Furthermore, they state that including additional particles in the computation has little effect on the results so that this calculation is equivalent to one including all-neighbor interactions (AN).

TABLE VII. Adiabatic elastic constants and elastic anisotropy of xenon derived from various theories. Values quoted for the elastic constants correspond to the curves plotted in Fig. 8. (NN) represents nearest-neighbor interactions. (AN) represents all-neighbor interactions.

Theory	Temp. (°K)	c_{11}	c_{12}	c_{44}	A	Ref.
			$(10^{10}$ dyn/cm^2)			
Central force (NN)	0	5.50	2.71	2.75	1.97	28
Central force (AN)	0	5.11	2.89	2.93	2.64	28
Three-body force (AN)	0	4.93	2.88	2.39	2.33	35
QH central force (NN)	78	4.56	2.39	2.05	1.89	24
	106	4.10	2.20	1.73	1.82	
SC central force (NN)	80	4.54	2.31	2.13	1.91	31
	120	3.97	2.08	1.76	1.86	
	160	3.64	2.00	1.48	1.80	
QH central force (AN)	30	4.95	2.87	2.78	2.67	36
	86	4.09	2.47	2.15	2.65	
	133	3.42	2.15	1.65	2.60	
	161	3.04	1.96	1.35	2.50	

The same lattice-dynamics calculations have been used to calculate adiabatic elastic constants for xenon[34] and the results are shown in Fig. 8. The agreement with our experimental values is excellent for all three elastic constants. Moreover, as pointed out in Ref. 34, the anharmonic corrections implied by the Monte Carlo calculations for argon would produce even better agreement with the experimental data. A comparison of the experimental and calculated values plotted in Fig. 8 indicates that, in calculating the elastic constants of rare-gas crystals such as xenon, it is necessary to include interactions beyond the range of nearest neighbors.

The elastic anisotropy $A = 2c_{44}/(c_{11} - c_{12})$ is a useful quantity for comparing various theories because it is independent of whether adiabatic or isothermal elastic constants are employed in calculating it [see Eqs. (24)]. Table VII gives the elastic anisotropy of xenon calculated from results of several different theories over a range of temperatures. It is immediately evident from Table VII that the elastic anisotropy for xenon is approximately 50% higher for the calculations including all-neighbor interactions than for those restricted to nearest-neighbor interactions only. Furthermore, both NN and AN

derivations exhibit little change in A throughout the full temperature range so that it is not unreasonable to expect the elastic anisotropy calculated at 0 °K to be comparable to the value at the melting point of the crystal. Indeed, in all cases the AN calculations are in good agreement with the experimental value of $A = 2.74 \pm 0.30$. The addition of three-body forces discussed by Zucker and Chell[35] produces a slightly lower anisotropy at 0 °K, but a value which does not seriously disagree with the present experiment.

VI. CONCLUDING REMARKS

The elastic constants of xenon single crystals have been determined by Brillouin spectroscopy with an accuracy of $\pm 3\%$. This is the first time that this technique has been used to study rare-gas crystals and the present experiment has produced some very interesting results. The adiabatic elastic constants obtained for xenon imply that rare-gas crystals are much more elastically anisotropic than previous ultrasonic measurements on argon have indicated. The high elastic anisotropy is consistent with theoretical predictions of the lattice dynamics of rare-gas crystals, but good agreement with the experimental value is found only for calculations of the elastic constants where all-neighbor interactions are included.

The present experiment has shown that Brillouin scattering is probably the best technique for studying the elastic properties of rare-gas single crystals. However, the measurements on xenon crystals covered a very limited temperature range just below the melting point. Further experimental measurements are necessary and desirable particularly at lower temperatures.

ACKNOWLEDGMENTS

[1]See review articles by B. L. Smith, Contemp. Phys. 11, 125 (1970); G. K. Horton, Am. J. Phys. 36, 93 (1968); G. Boato, Cryogenics 4, 65 (1964); G. I. Pollack, Rev. Mod. Phys. 36, 748 (1964); A. C. Hollis Hallett, in Argon, Helium and the Rare Gases, edited by G. A. Cook (Interscience, New York, 1961), Vol. I.

[2]See, for example, N. S. Gillis, N. R. Werthamer, and T. R. Koehler, Phys. Rev. 165, 951 (1968); M. L. Klein, G. K. Horton, and J. L. Feldman, ibid. 184, 968 (1969).

[3]O. G. Peterson, D. N. Batchelder, and R. O. Simmons, J. Appl. Phys. 36, 2682 (1965); D. L. Losee and R. O. Simmons, Phys. Rev. 172, 934 (1968).

[4]O. G. Peterson, D. N. Batchelder, and R. O. Simmons, Phys. Rev. 150, 703 (1966); D. N. Batchelder, D. L. Losee, and R. O. Simmons, ibid. 162, 767 (1967); 173, 873 (1968); A. O. Urvas, D. L. Losee, and R. O. Simmons, J. Phys. Chem. Solids 28, 2269 (1967); D. L. Losee and R. O. Simmons, Phys. Rev. 172, 944 (1968).

[5]H. R. Moeller and C. F. Squire, Phys. Rev. 151, 689 (1966).

[6]M. Gsänger, H. Egger, and E. Lüscher, Phys. Letters 27A, 695 (1968).

[7]G. J. Keeler and D. N. Batchelder, J. Phys. C 3, 510 (1970).

[8]W. B. Daniels, G. Shirane, B. C. Frazer, H. Umebayashi, and J. A. Leake, Phys. Rev. Letters 18, 548 (1967).

[9]J. A. Leake, W. B. Daniels, J. Skalyo, B. C. Frazer, and G. Shirane, Phys. Rev. 181, 1251 (1969).

[10]D. N. Batchelder, M. F. Collins, B. C. G. Haywood, and G. R. Sidney, J. Phys. C 3, 249 (1970).

[11]R. A. Cowley, Proc. Phys. Soc. (London) 90, 1127 (1967).

[12]R. S. Krishnan, Proc. Indian Acad. Sci. A41, 91 (1955).

[13]G. B. Benedek and K. Fritsch, Phys. Rev. 149, 647 (1966).

[14]J. Shaham, H. Kaplan, W. Low, and M. Foguel, Phys. Rev. Letters 24, 827 (1970).

[15]W. S. Gornall and B. P. Stoicheff, Solid State Commun. 8, 1529 (1970).

[16]For convenience the acoustic modes and the associated spectral components will be referred to as longitudinal and transverse. It should be understood, however, that significant admixtures of the mode polarizations occur depending on the direction of wave propagation in the crystal (see Ref. 13).

[17]See, for example, C. Kittel, Introduction to Solid State Physics (Wiley, New York, 1968), pp. 109–129.

[18]J. F. Nye, Physical Properties of Crystals (Clarendon, Oxford, 1957).

[19]J. R. Neighbours and C. S. Smith, J. Appl. Phys. 21, 1338 (1950).

[20]See C.-E. Fröberg, Introduction to Numerical Analysis (Addison-Wesley, Cambridge, Mass., 1965), p. 109.

[21]H. Goldstein, Classical Mechanics (Addison-Wesley, Cambridge, Mass., 1950), p. 107.

[22]J. R. Packard and C. A. Swenson, J. Phys. Chem. Solids 24, 1405 (1963).

[23]A. C. Sinnock and B. L. Smith, Phys. Letters 28A, 22 (1968); Phys. Rev. 181, 1297 (1969).

[24]C. Feldman, M. L. Klein, and G. K. Horton, Phys. Rev. 184, 910 (1969).

[25]G. Leibfried and W. Ludwig, in Solid State Physics, edited by F. Seitz and D. Turnbull (Academic, New York, 1961), Vol. 12, p. 275.

[26]V. G. Manzhelii, V. G. Gavrilko, and V. I. Kuchnev, Phys. Status Solidi 34, K55 (1969).

[27]K. Clusius and L. Riccoboni, Z. Physik. Chem. (Leipzig) B38, 81 (1937).

[28]T. H. K. Barron and M. L. Klein, Proc. Phys. Soc. (London) 85, 533 (1965).

[29]See, for example, Ph. Choquard, The Anharmonic Crystal (Benjamin, New York, 1967); H. Horner, Z. Physik 205, 72 (1967); N. R. Werthamer, Phys. Rev. B 1, 572 (1970); and Ref. 2.

[30]V. V. Goldman, G. K. Horton, and M. L. Klein, Phys. Rev. Letters 21, 1527 (1968); Phys. Letters 28A, 341 (1968).

[31]M. L. Klein (private communication).

[32]M. L. Klein, V. V. Goldman, and G. K. Horton, J. Phys. Chem. Solids 31, 2441 (1970).

[33]W. G. Hoover, A. C. Holt, and D. R. Squire, Physica 42, 388 (1969); 44, 437 (1969).

[34]A. C. Holt, W. G. Hoover, S. G. Gray, and D. R. Shortle, Physica 49, 61 (1970).

[35]I. J. Zucker and G. G. Chell, J. Phys. C 1, 1505 (1968).

[36]A. C. Holt (private communication).

Exciton Energy Levels in Wurtzite-Type Crystals*

Nunzio O. Lipari

Department of Physics and Materials Research Laboratory,
University of Illinois, Urbana, Illinois 61801

The exciton problem in wurtzite-type crystals is investigated taking into full account the structure of the valence bands. Using perturbation theory, after a proper rotation of the exciton Hamiltonian, we obtain analytical expressions for the exciton ground states originating from the Γ_9, Γ_7, and Γ_7 valence subbands. These expressions are valid for any value of the crystal field splitting. Results are given for CdSe and CdS and the agreement with experiment is good.

Structure due to excitons was first observed in II-VI wurtzite compounds by Gross and co-workers[1] and by Thomas and Hopfield.[2] Since then, many authors[3] have investigated direct excitons in these materials. From the theoretical point of view, however, little work has been done.

It is well known that crystals with diamond and zinc-blende lattices have valence-band states orig-

inating from atomic p states and that the maximum of the valence band is at $\vec{k} = 0$.[4] The valence bands of wurtzite-type materials also originate from atomic p states[5] but, because the symmetry is lower than that of the diamond and zinc-blende cases, the situation is more complicated. It is known, however, that the maximum is still exactly (or very nearly) at $\vec{k} = 0$. The minimum of the con-

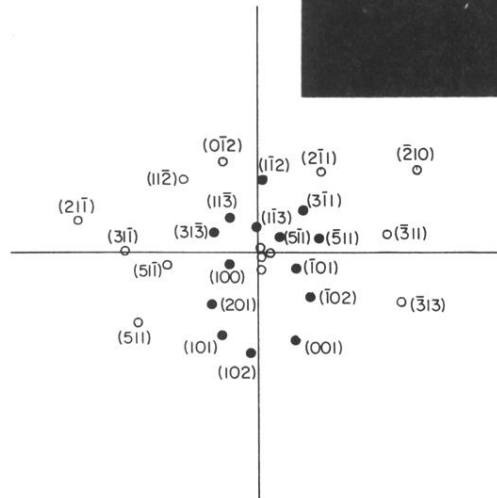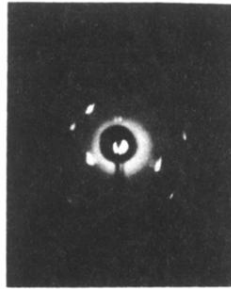$\theta = 26.0°$
$\phi = 239.0°$
$\chi = 123.0°$

FIG. 3. Laue diffraction photograph of a xenon single
crystal taken at a distance of 5.00 cm. Below it (on the
same scale) is the computed diffraction pattern that identi-
fied the orientation as (26°, 239°, 123°). The solid dots
correspond to those actually observed on the photograph.